Journal of Zhejiang University-SCIENCE A (Applied Physics & Engineering)
ISSN 1673-565X (Print); ISSN 1862-1775 (Online)
www.jzus.zju.edu.cn; www.springerlink.com
E-mail: jzus@zju.edu.cn

Rocking of a rigid block freestanding on a flat pedestal

Antonio GESUALDO[1], Antonino IANNUZZO[1], Michela MONACO[†‡2], Francesco PENTA[3]

[1]*Department of Structures for Engineering and Architecture, University of Naples Federico II, Naples 80125, Italy*

[2]*Department of Architecture and Industrial Design, University of Campania Luigi Vanvitelli, Aversa (Ce) 81031, Italy*

[3]*Department of Industrial Engineering, University of Naples Federico II, Naples 80125, Italy*

[†]E-mail: michela.monaco@unicampania.it

Received Feb. 5, 2017; Revision accepted June 30, 2017; Crosschecked Apr. 11, 2018

Abstract: The seismic protection of objects contained within museums is a topic of great interest, especially with reference to how they are displayed or stored. This problem is the same as that of a large class of non-structural components, such as mechanical and electrical hospital and laboratory equipment that could lose their functionality because of earthquakes. Statues and ceramics simply supported on the floor represent a significant set of case. In some cases, like the Bronzes of Riace, isolation systems have been developed. However, in general museum exhibits are not equipped with devices capable of mitigating the oscillations induced by possible earthquakes. The case study of a marble statue placed on a freestanding squat rigid pedestal is examined. The system of algebraic differential equations governing the problem has been derived and included in an ad-hoc numerical procedure. It is shown that the insertion of a squat rigid body with low frictional resistance at the lower interface with the floor, and high frictional resistance at the upper interface with the artifact significantly reduces the amplitude of the rocking response. As a result the artifact rocks without sliding on the rigid base that slides without rocking with respect to the floor. The numerical analysis performed can be a tool to help in the choice of the optimal friction values in the surfaces of the flat block, designed as a simple isolation system.

Key words: Rigid body; Isolation; Statues; Friction; Rocking dynamics
https://doi.org/10.1631/jzus.A1700061 **CLC number:** O32

1 Introduction

Early study on the rocking response of a rigid block supported on a base undergoing horizontal motion was presented by Housner (1963), who first established and solved the equations of motion of the rigid body. The study was devoted to the understanding of the behaviour of tall, slender structures subjected to ground motion. Only recently have studies addressed the issue of the contents of buildings in seismic areas, especially art objects in museums (Gesualdo et al., 2016a). The seismic safety of artifacts is a research field of great interest, being part of research and policy in the more general field of Cultural Heritage, and has attracted several local government and European research grants (Erdik et al., 2010).

The first study related to the seismic safeguarding of art objects is that by Agbabian et al. (1991). It was developed in the framework of a research program sponsored by the Getty Museum in Malibu, California, USA. In that study a wide range of objects was classified according to their form and method of exhibiting. Analytical and experimental techniques were combined in order to evaluate the possible damage risk due to earthquakes. One of the problems examined concerned the safeguarding of freestanding vases and statues. The problem involves limitation of excessive motion of rigid bodies under earthquake excitation. Since the late XIX century the behaviour

‡ Corresponding author
ORCID: Antonio GESUALDO, https://orcid.org/0000-0002-7063-8064; Michela MONACO, https://orcid.org/0000-0001-7895-7089

of many objects such as hospital devices, statues, and storage tanks has been studied in this framework (Penta et al., 2014). Six basic conditions (Augusti and Sinopoli, 1992) have been distinguished: rest, slide, rock, slide-rock, free flight, and impact. Despite their familiarity and apparent simplicity, the motions of rigid bodies in response to earthquake excitations pose extremely difficult problems when exact solutions are sought (Voyagaki et al., 2014). Shenton (1996) showed that the motion of a rigid object simply supported on a uniformly accelerating rigid plane depends not only on the object shape and the base acceleration, but also on the friction coefficient. According to the author the friction required to initiate a rocking mode increases with ground acceleration. It has been shown (Monaco et al., 2014) that the range of a sliding-rock is larger in the case of harmonic excitation. The role of friction and its influence on the quality of motion have also been considered (Sinopoli, 1997).

A rigid structure placed on a shaking base may enter a rocking motion that occasionally results in overturning (Guadagnuolo and Monaco, 2009). In some cases an appropriate constitutive model of the structure is an essential tool for the protection of the museum building (Gesualdo and Monaco, 2015; Cennamo et al., 2017), but in the case of art objects the development of a designed exhibit system is needed (Chierchiello et al., 2015). In the first study performed in Japan (Ishiyama 1982), a computer simulation showed that the horizontal velocity as well as the acceleration must be taken into account as criteria for overturning. Since the rocking response of a rigid body to base motion is sensitive to parameters defining the geometry of the body and details of base motion (Housner, 1963), a limited number of simulated ground motions can produce curves giving the probability of the body to overturn (Yim et al., 1980). The simplest of the mathematical models that has received notable attention in the past has been the planar rocking of rigid rectangular blocks under harmonic base motions (Newmark, 1965; Spanos and Koh, 1984) although also the influence of the ground motion properties has been analyzed since the first years of 1980s (Yim et al., 1980; Purvance et al., 2008). In the harmonic problem, the non-linearity arises not only in the displacements but also in the dissipation of energy due to impacts. Using two types of base motions, 50 artificial earthquakes simulated in a way identical to that of Yim et al. (1980) and 75 real earthquakes, Shao and Tung (1999) showed that real earthquakes give a lower probability of overturning than simulated earthquakes. The rocking response of a rigid body to harmonic shaking as well to simulated earthquake motions has been deduced both numerically and by laboratory experiments (Aslam et al., 1980; Hogan, 1989). Hogan (1989) examined stability boundaries and the evolution of motion with different starting conditions.

The influence of the slenderness parameter has been much investigated (Psycharis et al., 2000; Makris and Vassiliou, 2012). Recent studies (Prieto and Lourenço, 2005) have tried to unify the piecewise formulation of Housner, with the same hypothesis of a large friction coefficient. The traditional piecewise formulation is replaced by a single ordinary differential equation, and damping effects are no longer introduced by means of a coefficient of restitution, but are understood as the presence of impulsive forces. The results are in agreement with the classical formalism, and can be set as a direct analogy with either a two-body central problem in the complex plane, or an inverted pendulum through simple variable transformations. Unfortunately, these elegant formulations are unsuitable when rocking motion is to be avoided and sliding motion is welcome, as in the case of artifacts (Gesualdo et al., 2014). A limited number of studies take into account sliding motion (Voyagaki et al., 2012), since in large part the friction coefficient between the block and base is assumed sufficiently large to prevent sliding. In the study of Kounadis (2015), the combination of rocking and sliding for the simple block case is reported. In the slender block problem closed-form solutions are derived.

Some studies on the response of this system have revealed the presence of a rich variety of non-linear resonances and even the possibility of the response becoming chaotic. Tackling analytically the equations of motion for real earthquake ground motions is not a trivial task even for very simple waveforms (Konstantinidis and Makris, 2010). A range of idealized ground acceleration pulses expressed by a generalized function controlled by a single shape parameter has been considered in (Voyagaki et al., 2014). The problem is treated analytically by means of linearized equations of motion under the assumption of slender block geometry and rocking without sliding. Peak rocking response and overturning criteria for different

waveforms are presented in terms of dimensionless closed-form expressions and graphs. Recent attempts have been made to derive equivalence between the single rocking block and various rocking mechanisms, in order to give an indication for real structures (de Jong and Dimitrakopoulos, 2014).

The problem becomes more complex when the behaviour of two stacked rigid bodies is examined: the highly nonlinear formulation needs some simplifying assumptions (Psycharis, 1990). In the case examined by Spanos et al. (2001) large friction is considered to prevent sliding. In the case of a museum artifact, rocking behaviour is not a desired condition, but sliding should be sought (Gesualdo et al., 2016b). In particular cases, like the Riace Bronzes, isolation systems have been developed, while in general, museum exhibits are not equipped with devices capable of mitigating the oscillations induced by possible earthquakes (Gesualdo et al., 2017). A simple and low cost system should be developed in order to protect small art objects (Di Egidio and Contento, 2009).

In this study, the last problem is addressed: the dynamic behaviour of two stacked rigid bodies is considered. The two rigid bodies represent the slender artifact and the squat rigid base inserted between the floor and the artifact. First, the dynamic equations governing the motion of the single block are derived. Sliding and rocking motion are taken into account. Then, the equations of dynamic behaviour of two superimposed rigid blocks under harmonic base motion are deduced and solved by means of a purpose-built numerical procedure. Reference is made to two case studies.

The results could be useful in the determination of the optimal frictional coefficient of the interface between the art object and the squat base. The analyses show that the proposed system results in a decrease of oscillation amplitude and in some cases avoids the overturning.

2 Rocking and sliding response of a single block

2.1 Rocking

The pure rocking motion of one rigid block is examined. A symmetric rigid block with aspect ratio, B/H simply supported on a moving plane with acceleration $\ddot{x}_g(t)$ is shown in Fig. 1, where h is the half height and G represents the mass centroid of the block. The static friction coefficient μ_s takes into account the amount of force that is needed to originally initiate the sliding motion.

The force needed to keep the object sliding is proportional to the kinetic friction coefficient μ_k, with $\mu_s>\mu_k$. The block can rotate alternatively around the two base corners O and O' with rotation angle θ, clockwise positive (Fig. 2). The motion is described with reference to the target point P, whose position vectors are $\boldsymbol{r}_P^{(1)}$ and $\boldsymbol{r}_P^{(2)}$ with respect to O' and O. Energy is lost only during impact, when the angle of rotation reverses (Moreau and Panagiotopoulos, 1988). Reference is made to the classical approach of the dynamics of an inverted pendulum under impulsive excitations (Housner, 1963).

The velocity after a perfect plastic and centered impact is related to the pre-impact velocity field by means of a restitution coefficient r, assumed constant during the motion. The angular velocity of the block after the impact is given by

$$\dot{\theta}^+(t) = r\,\dot{\theta}^-(t), \tag{1}$$

where t is the time. In these hypotheses the conservation of angular momentum about point O' just before and just after the impact is

$$\left(I_o - 2mrb\sin\alpha\,\dot{\theta}^-(t)\right) = I_o\,\dot{\theta}^+(t), \tag{2}$$

where I_o is the polar inertia moment with respect to the two points O and O', m is the mass of the block, b is the half width of the block, and α is the zenithal angle of centroid. The value of r for a rectangular block can be derived by a combination of Eqs. (1) and (2):

$$r = 1 - \frac{3}{2}\sin^2\alpha, \quad 0 < r < 1. \tag{3}$$

When the rotation axis instantaneously moves between O and O' the coefficient of restitution is a measure of the energy lost during the impact. Rocking motion is present when the static friction with the base plane is so great as to prevent sliding. Adopting the notation by Shenton (1996), let f_x and f_y be the horizontal and vertical reactions at the tip O' of the block, respectively, and at all times the rocking motion holds true if:

$$\left|f_x\right| \le \mu_s f_y. \tag{4}$$

In other words, starting from an equilibrium configuration of the system and given the condition Eq. (4), the angular momentum of inertial forces is greater than that due to gravity. The rocking motion, according to the D'Alembert principle, is governed by the following set of differential equations (DEs):

$$\begin{cases} I_{O'}\,\ddot{\theta}(t) + mgR\sin\left(-\alpha-\theta(t)\right) \\ \qquad = -m\ddot{x}_g(t)\,R\cos\left(-\alpha-\theta(t)\right), & \theta(t)<0, \\ I_O\,\ddot{\theta}(t) + mg\,R\sin\left(\alpha-\theta(t)\right) \\ \qquad = -m\ddot{x}_g(t)\,R\cos\left(\alpha-\theta(t)\right), & \theta(t)>0, \\ \dot{\theta}^+(t) = r\,\dot{\theta}^-(t), & \theta(t)=0, \end{cases} \tag{5}$$

where R is the length of the segment OG or $O'G$, $\ddot{x}_g(t)$ is the horizontal base acceleration, I_O=$I_{O'}$ is the polar inertia moment with respect to the two points O and O' and the rocking motion starts when $\left|\ddot{x}_g(t)\right| > gb/h$, being g the acceleration due to gravity. The first two ordinary nonlinear differential equations are relative to the rotation motion around O and O', and the third algebraic equation relates the two angular velocities in O and O' and holds true at the impact instant only. The angle α=arctan(b/h) takes into account the slenderness of the block. By the signum function:

$$\operatorname{sgn}\left(\theta(t)\right) = \begin{cases} +1, & \theta(t)>0, \\ -1, & \theta(t)<0, \end{cases}$$

the system Eq. (5) can assume the following form:

$$\begin{aligned} &\frac{I_o}{mR}\ddot{\theta}(t) + g\operatorname{sgn}\left(\theta(t)\right)\sin\left(\alpha-\operatorname{sgn}\left(\theta(t)\right)\theta(t)\right) \\ &\quad = -\ddot{x}_g(t)\cos\left(\alpha-\operatorname{sgn}\left(\theta(t)\right)\theta(t)\right), \quad \theta(t)\neq 0, \\ &\dot{\theta}^+(t) = r\,\dot{\theta}^-(t), \quad \theta(t)=0. \end{aligned} \tag{6}$$

The numerical solution of Eq. (6) may be put more conveniently in terms of a key point displacement, considering two reference systems with origin in the two rotation points O and O', namely $\mathcal{R}_1$={O, x, y} for $\theta(t)$>0 and $\mathcal{R}_2$={O', x', y'} for $\theta(t)$<0.

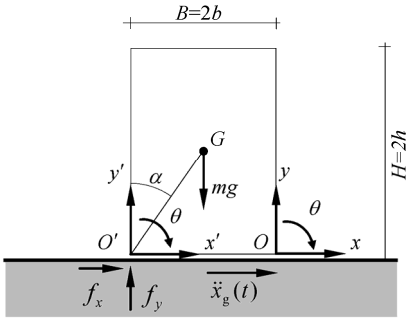

Fig. 1 Single rocking block

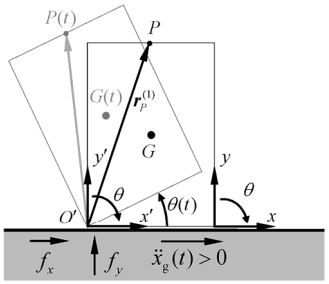

(a)

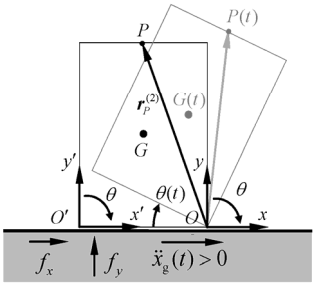

(b)

Fig. 2 Reference systems for the single rocking block in rocking for $\theta(t)$<0 (a) and $\theta(t)$>0 (b)

Let $\theta(t)$ be the rotation function. The position of the point P at time t in the two frame systems described above is related to the position vector at the starting time:

$$\begin{cases} \boldsymbol{r}_P^{(1)} = \begin{bmatrix} x_P^{(1)} \\ y_P^{(1)} \end{bmatrix}, & \theta(t)<0, \\ \boldsymbol{r}_P^{(2)} = \begin{bmatrix} x_P^{(2)} \\ y_P^{(2)} \end{bmatrix}, & \theta(t)>0, \end{cases} \tag{7}$$

so that the actual position of the point P is given by the rotation matrix $\boldsymbol{R}\circ\theta(t)$ applied on $\boldsymbol{r}_P^{(1)}$ and $\boldsymbol{r}_P^{(2)}$:

$$\begin{cases} OP(t) = \boldsymbol{R} \circ \theta(t)\, \boldsymbol{r}_P^{(1)}, & \theta(t) > 0, \\ O'P(t) = \boldsymbol{R} \circ \theta(t)\, \boldsymbol{r}_P^{(2)}, & \theta(t) < 0, \end{cases} \tag{8}$$

where the rotation matrix $\boldsymbol{R}$, being $SO(2)$ the orthogonal group of matrices with $\det(\boldsymbol{R})=1$, is

$$\boldsymbol{R} \circ (\cdot) = \begin{bmatrix} \cos(\cdot) & \sin(\cdot) \\ -\sin(\cdot) & \cos(\cdot) \end{bmatrix}. \tag{9}$$

From Eq. (8) the acceleration is derived as

$$\begin{cases} \dfrac{\partial^2}{\partial t^2} OP(t) = \dfrac{\partial^2}{\partial t^2} [\boldsymbol{R} \circ \theta(t)]\, \boldsymbol{r}_P^{(1)}, & \theta(t) > 0, \\ \dfrac{\partial^2}{\partial t^2} O'P(t) = \dfrac{\partial^2}{\partial t^2} [\boldsymbol{R} \circ \theta(t)]\, \boldsymbol{r}_P^{(2)}, & \theta(t) < 0. \end{cases} \tag{10}$$

After some manipulation Eq. (10) can be rewritten as follows:

$$\begin{cases} \dfrac{\partial^2}{\partial t^2} OP = \\ \left[\ddot{\theta}(t) \partial \boldsymbol{R} \circ \theta(t) - \dot{\theta}^2(t)\, \boldsymbol{R} \circ \theta(t) \right] \boldsymbol{r}_P^{(1)}, & \theta(t) > 0, \\ \dfrac{\partial^2}{\partial t^2} O'P = \\ \left[\ddot{\theta}(t) \partial \boldsymbol{R} \circ \theta(t) - \dot{\theta}^2(t)\, \boldsymbol{R} \circ \theta(t) \right] \boldsymbol{r}_P^{(2)}, & \theta(t) < 0, \end{cases} \tag{11}$$

where the first derivative of the rotation matrix belongs to the orthogonal group of matrices with unit determinant:

$$\partial \boldsymbol{R} \circ (\cdot) = \begin{bmatrix} -\sin(\cdot) & \cos(\cdot) \\ -\cos(\cdot) & -\sin(\cdot) \end{bmatrix} \in SO(2).$$

The horizontal component of relative acceleration can be deduced by Eq. (11):

$$\ddot{x}(t) = \begin{cases} \dfrac{\partial^2}{\partial t^2} OP \cdot \boldsymbol{i}, & \theta(t) > 0, \\ \dfrac{\partial^2}{\partial t^2} O'P \cdot \boldsymbol{i}, & \theta(t) < 0, \end{cases}$$

where $\boldsymbol{i}$ is the unit vector of the x axis. The horizontal acceleration $\ddot{x}(t)$ can be put in the explicit form:

$$\ddot{x}(t) = \begin{cases} -[x_P^{(1)} \cos(\theta(t)) + y_P^{(1)} \sin(\theta(t))]\, \dot{\theta}(t) \\ \quad + [-x_P^{(1)} \sin(\theta(t)) + y_P^{(1)} \cos(\theta(t))]\, \ddot{\theta}(t), & \theta(t) > 0, \\ -[x_P^{(2)} \cos(\theta(t)) + y_P^{(2)} \sin(\theta(t))]\, \dot{\theta}(t) \\ \quad + [-x_P^{(2)} \sin(\theta(t)) + y_P^{(2)} \cos(\theta(t))]\, \ddot{\theta}(t), & \theta(t) < 0. \end{cases} \tag{12}$$

The absolute acceleration

$$\ddot{x}_{\mathrm{a}}(t) = \ddot{x}_{\mathrm{g}}(t) + \ddot{x}(t) \tag{13}$$

is the sum of the base and block accelerations.

2.2 Sliding

The configuration of the block in the case of sliding motion can be characterized by the translation of a generic point of the block with respect to the base (Newmark, 1965; Conte and Dente, 1989). The friction force is a function of the vertical forces applied to the block and is opposite to the motion.

Starting from an equilibrium configuration, sliding motion begins when the maximum horizontal force due to the static friction coefficient is attained (Voyagaki et al., 2012).

With reference to the scheme of Fig. 3, the governing equations are

$$\begin{aligned} &|\ddot{x}_{\mathrm{g}}(t)| > g\mu_{\mathrm{s}}, \\ &\ddot{x}_{\mathrm{g}}(t) + \ddot{x}(t) = -\mathrm{sgn}(\dot{x}(t))\, g\mu_{\mathrm{k}}. \end{aligned} \tag{14}$$

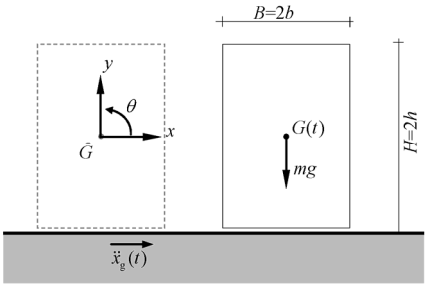

Fig. 3 Single sliding block

Starting from the instant in which the friction contact force is exceeded by the inertial forces related to Eq. (13), the differential equation of sliding Eq. (14) is integrated in the numerical procedure until the relative velocity $\dot{x}(t)$ is nonzero. When the

velocity becomes null the block is in relative equilibrium with the base (rest) until the external force attains a value able to reactivate the sliding motion.

3 Dynamic analysis of double stacked blocks

The analysis of rocking behaviour is a key aspect of safety assessment and the maintenance of artifacts, like statues and vases, since the rocking itself can be the cause of damage at the base of the object, due to impact with the support. By seismic excitation, a freestanding object may in fact enter a rocking state which would cause overturning, so that often the sliding is desirable, given the possibility of evaluating relative displacements to avoid collisions.

The prevention of seismic damage can be affected by base isolation devices as in the cases of the Bronzes of Riace (Fig. 4a), but this type of protection is expensive and can only really be used for particularly valuable objects. In the majority of cases, museum exhibitions are not equipped with isolation devices for every single contained object. For the Bronzes the protection system is composed of two marble blocks connected by spheres and dissipative devices made by stainless steel cables for horizontal displacement limitation and recentering, while a vertical isolation element is located in the upper block (de Canio, 2012) (Fig. 4b).

This study presents the theoretical and numerical bases of a simple and low cost isolation system to protect small art objects. This is key since smaller artifacts are also the more prone to overturning since the rocking response is highly influenced by the size of the object. The insertion of a further rigid body between the moving base and the statue can reduce the effect of base motion due to earthquakes.

It is possible to develop surfaces with an a priori fixed friction coefficient so that the oscillation at the base of the art object can be reduced and in some cases avoided, thus controlling the value of the friction coefficient between the contact surfaces. In the following, the results of an analysis made by means of a purpose-built numerical procedure are presented.

This study is the first step toward the choice of the optimal friction coefficient to be created in these inserted surfaces. The problem studied in this section concerns the motion of two superimposed blocks of different aspect ratios: a top slender block placed on a flat one, both on a moving base.

The hypotheses are made in order to represent the real situation of a marble statue placed on a flat rigid pedestal freestanding on a moving floor (Fig. 4c). The problem is mixed: the possible motion for the lower flat block is the only sliding one, while rocking is the only possible motion for the stacked slender block. The differential equations governing the problem have been derived and included in the numerical procedure developed with Mathematica© (Wolfram, 2003).

3.1 Formulation of the problem

The geometrical characteristics of the two stacked blocks are shown in Fig. 5. The lower flat block is tagged with index 1 and the top slender element with index 2.

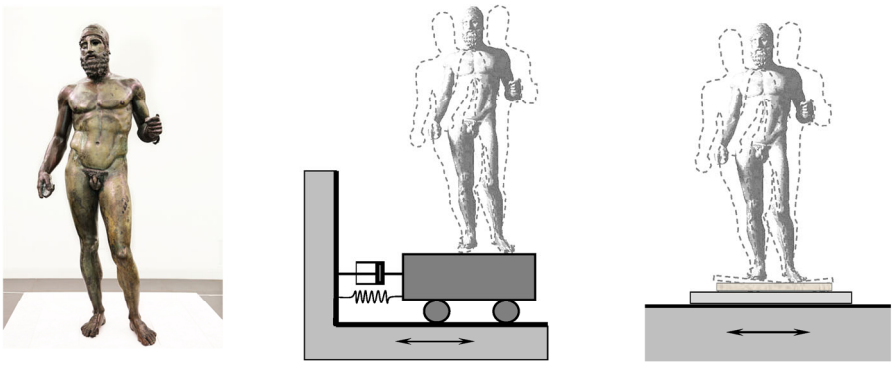

Fig. 4 Freestanding statue (a), isolation system (b), and single flat block (c)

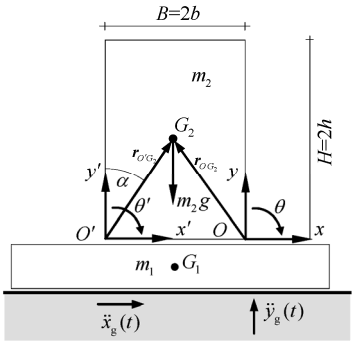

Fig. 5 Double blocks at rest position

The dimensions of the lower block can only allow sliding motion and a rocking one is possible for the superimposed block 2 due both to the high friction coefficient between blocks 1 and 2 and to the slenderness of block 2. As a consequence, the system has two degrees of freedom, namely the rotation θ (clockwise positive) of block 2 and the centroid position x_{G_1} of block 1. Assuming m_1 and m_2 as the masses of the two blocks whose center of masses are G_1 and G_2, respectively, $M=m_1+m_2$ is the total mass of the system and $x_g(t)$ and $y_g(t)$ are the base motion components.

Let $\boldsymbol{r}_{O'G_2}$ and $\boldsymbol{r}_{OG_2}$ be the position vectors of G_2 relative to O' and O in the initial configuration (Fig. 5). Their components in the two Cartesian reference systems $\mathcal{R}_1$ and $\mathcal{R}_2$ are given by

$$\boldsymbol{r}_{O'G_2}=\begin{bmatrix} R\sin\theta \\ R\cos\theta \end{bmatrix}, \qquad \boldsymbol{r}_{OG_2}=\begin{bmatrix} R\sin\theta \\ -R\cos\theta \end{bmatrix}. \tag{15}$$

The hypothesis of sliding motion for block 1 leads to a null vertical component of its relative motion with respect to the base. The position of the center of mass G_1 is

$$\boldsymbol{x}_{G_1}(t)=\begin{bmatrix} x_{\mathrm{g}}(t)+x_{G_1}(t) \\ y_{\mathrm{g}}(t) \end{bmatrix}$$

and that of G_2 is

$$\begin{cases} \boldsymbol{x}'_{G_2}(t)=\boldsymbol{x}_{G_1}(t)+\boldsymbol{R}\circ\theta(t)\,\boldsymbol{r}_{O'G_2}, & \theta(t)<0, \\ \boldsymbol{x}_{G_2}(t)=\boldsymbol{x}_{G_1}(t)+\boldsymbol{R}\circ\theta(t)\,\boldsymbol{r}_{OG_2}, & \theta(t)>0, \end{cases}$$

so that the actual position $P(t)$ of the key point P is

$$\begin{cases} O'P(t)=\boldsymbol{R}\circ\theta(t)\,\boldsymbol{r}_P^{(1)}, & \theta(t)<0, \\ OP(t)=\boldsymbol{R}\circ\theta(t)\,\boldsymbol{r}_P^{(2)}, & \theta(t)>0, \end{cases}$$

where $\boldsymbol{R}\circ\theta(t)$ is the rotation matrix (Eq. (9)) that takes into account the rocking motion of block 2, and the position vectors $\boldsymbol{r}_P^{(1)}$ and $\boldsymbol{r}_P^{(2)}$ are represented in Fig. 6. The total kinetic energy of the system is

$$T(t)=T_1(t)+T_2(t),$$

with $T_1(t)$ and $T_2(t)$ the kinetic energies of blocks 1 and 2, respectively:

$$\begin{cases} T_1(t)=\dfrac{1}{2}m_1\,\dot{\boldsymbol{x}}_{G_1}\cdot\dot{\boldsymbol{x}}_{G_1}, & \theta(t)<0, \\ T_2(t)=\dfrac{1}{2}\left[J_{G_2}\dot{\theta}^2(t)+m_2\,\dot{\boldsymbol{x}}'_{G_2}(t)\cdot\dot{\boldsymbol{x}}'_{G_2}(t)\right], & \theta(t)<0, \\ T_1(t)=\dfrac{1}{2}m_1\,\dot{\boldsymbol{x}}_{G_1}\cdot\dot{\boldsymbol{x}}_{G_1}, & \theta(t)>0, \\ T_2(t)=\dfrac{1}{2}\left[J_{G_2}\dot{\theta}^2(t)+m_2\,\dot{\boldsymbol{x}}_{G_2}(t)\cdot\dot{\boldsymbol{x}}_{G_2}(t)\right], & \theta(t)>0, \end{cases} \tag{16}$$

where J_{G_2} is the centroid moment of inertia of block 2. The potential energy of the two blocks is given by

$$V(t)=V_1(t)+V_2(t),$$

with $V_1(t)$ and $V_2(t)$ the potential energies of blocks 1 and 2, respectively:

$$\begin{cases} V_1(t)=m_1g\,\boldsymbol{x}_{G_1}\cdot\boldsymbol{j}, & \theta(t)<0, \\ V_2(t)=m_2g\,\boldsymbol{x}'_{G_2}\cdot\boldsymbol{j}, & \theta(t)<0, \\ V_1(t)=m_1g\,\boldsymbol{x}_{G_1}\cdot\boldsymbol{j}, & \theta(t)>0, \\ V_2(t)=m_2g\,\boldsymbol{x}_{G_2}\cdot\boldsymbol{j}, & \theta(t)>0, \end{cases} \tag{17}$$

where $\boldsymbol{j}$ is the unit vector of the y axis. The friction force at the base of block 1 during the sliding movement is given by

$$F_{x,\mathrm{friction}}=-\mu_{\mathrm{k}}M(g+\ddot{y}_{\mathrm{g}}(t))\,\ddot{x}_{\mathrm{g}}(t)\,\mathrm{sgn}(\dot{x}_{\mathrm{g}}(t)), \tag{18}$$

so that the Lagrangian formulation of the problem states, as developed in (Voyagaki et al., 2013):

$$L(t)=T(t)-V(t), \tag{19}$$

with the two Lagrangian parameters:

$$q_1(t)=x_{G_1}(t), \quad q_2(t)=\theta(t).$$

The motion is governed by two differential equations derived by the Euler-Lagrange relation:

$$\frac{\partial^2 L(t)}{\partial t\partial \dot{q}_k}-\frac{\partial L(t)}{\partial q_k}=Q_k(t), \quad k=1,2, \tag{20}$$

where $Q_k(t)$ is the generalized non-conservative force dual to $q_k(t)$. The system assumes two different expressions according to the sign of $\theta(t)$. In view of Eqs. (16)–(20), the DEs can be expressed as

$$\begin{cases} J_O\ddot{\theta}(t)-m_2R\cos(\alpha-|\theta|)(\ddot{x}_g(t)+\ddot{x}_{G_1}(t)) \\ \quad +m_2Rg\,\mathrm{sgn}(\theta(t))\sin(\alpha-|\theta|)=0, & \theta(t)\neq 0, \\ M(\ddot{x}_g(t)+\ddot{x}_{G_1}(t))+\mathrm{sgn}(\theta(t))\{-m_2R[\sin(\alpha-|\theta|)\dot{\theta}^2(t) \\ \quad -\cos(\alpha-|\theta|)\ddot{\theta}(t)]+M\mu_k g\}=0, & \theta(t)\neq 0, \\ \dot{\theta}^+(t)=r\dot{\theta}^-(t), & \theta(t)=0, \end{cases} \tag{21}$$

where in a more simple form, $J_O=J_{G_2}$ is the centroid moment of inertia of block 2. The motion problem Eq. (21) is composed of two ordinary nonlinear differential equations and a single algebraic one, which involves the pre-and-post-impact angular velocity of the top block during the rocking motion. It is worth noting that uncoupling the two differential equations is not possible. The DEs in Eq. (21) govern the motions of the two blocks, while the rocking of the top block when the flat block is at rest with respect to the ground is governed by

$$\begin{aligned} &J_O\ddot{\theta}(t)-m_2R\cos(\alpha-|\theta|)\ddot{x}_g(t) \\ &\quad +m_2Rg\,\mathrm{sgn}(\theta(t))\sin(\alpha-|\theta|)=0, \end{aligned} \tag{22}$$

derived from Eq. (21) with the condition $q_1(t)=x_{G_1}(t)=0$. Eq. (22), analogous to Eq. (14) with the condition $\theta(t)=0$, describes the sliding motion of the two blocks:

$$\ddot{x}_g(t)+\ddot{x}_{G_1}(t)=-\mathrm{sgn}(\dot{x}_{G_1}(t))\mu_k g. \tag{23}$$

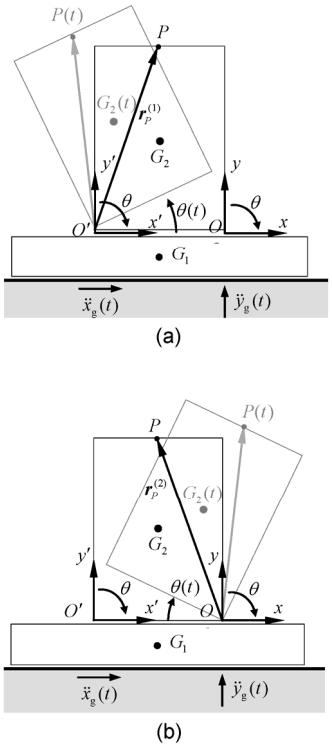

Fig. 6 Double blocks with upper block in rocking for $\theta(t)<0$ (a) and $\theta(t)>0$ (b)

The numerical procedure implemented in Mathematica© takes into account the only sliding motion for the lower block (i.e. a rigid flat pedestal), so that its mass is the only necessary mechanical parameter. The top slender block (in this case an anthropomorphic statue) can undergo rocking motion and the procedure involves the aspect ratio B/H. Given the geometrical conditions, at the starting point the two blocks are at rest with respect to the moving base, until Eq. (21) or (22) is activated according to the mechanical parameters involved.

The analysis of the dynamic system begins with the evaluation of the type of motion related to the base acceleration. Three possible patterns of motion have been examined (Fig. 7):

(a) Rocking of the top block with base block at rest with respect to the ground;

(b) Sliding motion of the two blocks as one rigid body;

(c) Combined motion patterns: rocking of the top block and sliding of the lower one.

The conditions for the activation of the motion (a) are given by

$$\begin{cases}\ddot{x}_{\mathrm{g}}(t) < \mathrm{sgn}(\dot{x}_{\mathrm{g}}(t))\,\mu_{\mathrm{k}} g, \\ \ddot{x}_{G_2}(t)\,h > gb. \end{cases} \tag{24}$$

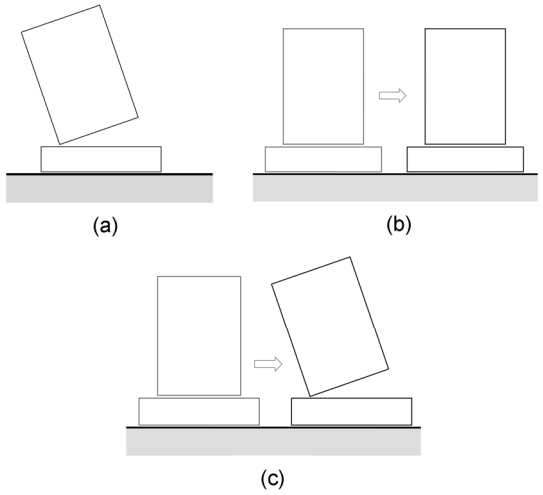

Fig. 7 Possible patterns of motion: (a) only rocking of the upper block; (b) sliding of the two blocks; (c) sliding of the lower block and rocking of the top one

The time t_{a} is the instant at which

$$\ddot{x}_{G_2}(t_{\mathrm{a}})\,h = gb. \tag{25}$$

It corresponds to the change of motion to range (b), whose conditions for the activation are given by

$$\begin{cases}\ddot{x}_{\mathrm{g}}(t) > \mathrm{sgn}(\dot{x}_{\mathrm{g}}(t))\,\mu_{\mathrm{k}} g, \\ \ddot{x}_{G_2}(t)\,h < gb. \end{cases} \tag{26}$$

The balance of the friction force with inertial forces corresponds to the time t_{b} in which

$$\ddot{x}_{\mathrm{g}}(t_{\mathrm{b}}) = \mathrm{sgn}(\dot{x}_{\mathrm{g}}(t_{\mathrm{b}}))\,\mu_{\mathrm{k}} g. \tag{27}$$

The conditions for the activation of the motion (c) are given by

$$\begin{cases}\ddot{x}_{\mathrm{g}}(t) > \mathrm{sgn}(\dot{x}_{\mathrm{g}}(t))\,\mu_{\mathrm{k}} g, \\ \ddot{x}_{G_2}(t)\,h > gb. \end{cases} \tag{28}$$

In general, the motion (a) lasts until the ground acceleration does not allow the overcoming of the static friction force at base interface.

The transition of motion from (a) to (c) occurs when

$$\begin{aligned} M\,\ddot{x}_{\mathrm{g}}(t) - m_2 R\,\mathrm{sgn}(\theta(t))[\sin(\alpha - |\theta(t)|)\,\dot{\theta}^2(t) \\ -\cos(\alpha - |\theta(t)|)\,\ddot{\theta}(t)] \geq \mathrm{sgn}(\theta(t))\,M\,\mu_{\mathrm{s}} g. \end{aligned} \tag{29}$$

Eq. (26) corresponds to Eq. (21) substituting the kinematic friction coefficient with the static one and $x_{G_1}(t) = 0 \rightarrow \ddot{x}_{G_1}(t) = 0$.

The inertial forces due to the ground acceleration $\ddot{x}_{\mathrm{g}}(t)$ and those due to the rocking of block 2 are involved in Eq. (27) with a term containing $\dot{\theta}^2(t)$ and another containing $\ddot{\theta}(t)$ which are respectively projections on the *x*-axis of the centripetal and tangential interactions through the contact point *O* or *O*′. The sliding motion of block 1 stops when $\dot{q}_1(t) = \dot{x}_{G_1}(t) = 0$.

The flow chart of the numerical routine is shown in Fig. 8, where the conditions for the integration of DEs governing the problem are shown schematically. A frequent circumstance involves the activation of the rocking of block 2 (left flow lines in the diagram): the

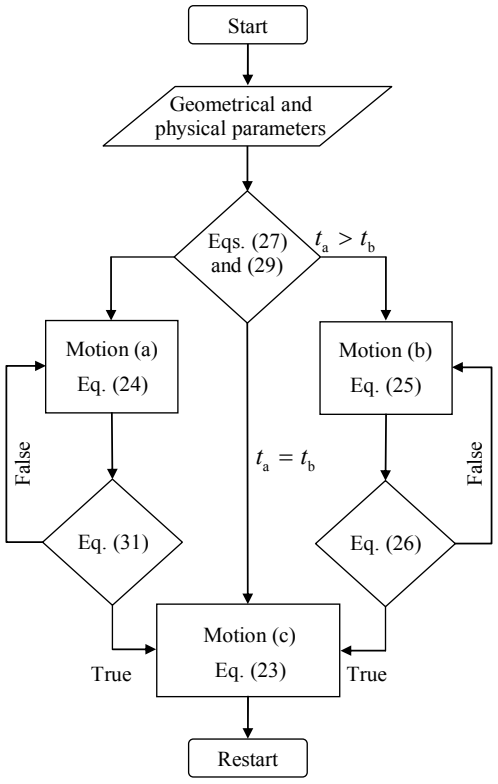

Fig. 8 Flow chart of the numerical routine

differential equation of rocking (Eq. (22)) is integrated until conditions for sliding (Eq. (27)) are attained, so that the system (Eq. (21)) is integrated until the velocity of block 1 with respect to the ground is null. From this point on the program the loop can restart and the procedure is able to choose the right motion according the dynamic conditions involved. In the examined cases Eq. (22) is activated before the static friction force between the flat block and the ground is exceeded. Only in this last case does the flat block initiate sliding.

3.2 Case studies

Several results considering the two-block system with harmonic ground motion are described below. Where possible the vertical scale is homogeneous to allow comparisons. The numerical parameters of motion common to all the examined cases are given in Table 1, while Table 2 contains the variable motion parameters and the correspondence to the figure diagrams. The first set of analyses (Figs. 9 and 10) is developed in the case of increasing slenderness.

Fig. 9a shows the behaviour of the two superimposed blocks with aspect ratio 0.5. Graph (a.1) represents the displacement of the flat block and graph (a.2) gives the rotation of the superimposed slender block. In graph (a.3) the behaviour of the slender block without the interposition of the flat one is depicted. Fig. 9b shows time histories related to a different slenderness (aspect ratio 0.33), in the same

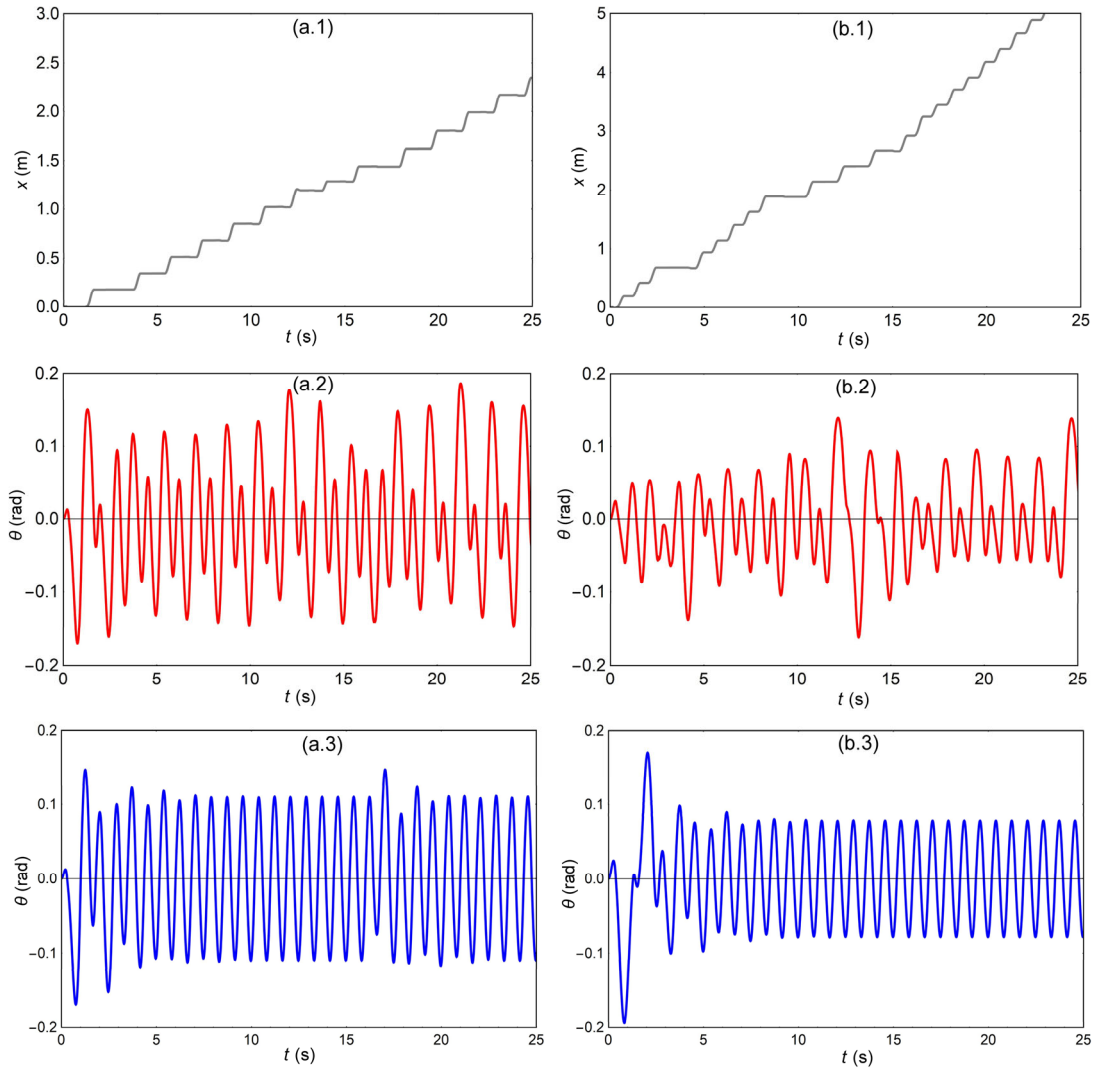

Fig. 9 Behaviour of the flat block (a.1, b.1), the stacked slender block (a.2, b.2), and the slender block alone (a.3, b.3) for varying *B*/*H*

Table 1 Motion parameters common to all analyses

μ_s	μ_k	B (m)	m_1 (kg)	r	f (Hz)	A (m/s^2)	ω (s^{-1})	$\ddot{x}(t)$
0.40	0.30	1	1	0.8	1.2	6.75	7.53	$A\cos(\omega t)$

f, A, and ω are the frequency, amplitude, and angular frequency of base excitation

Table 2 Variable motion parameters for the analyses

Data	m_2 (kg)	H (m)	Number of cycles	Data	m_2 (kg)	H (m)	Number of cycles
Fig. 9a	1	2	30	Fig. 11a	2	4	24
Fig. 9b	1	3	30	Fig. 11b	3	4	24
Fig. 10a	1	4	30	Fig. 12a	4	4	24
Fig. 10b	1	5	30	Fig. 12b	6	4	24

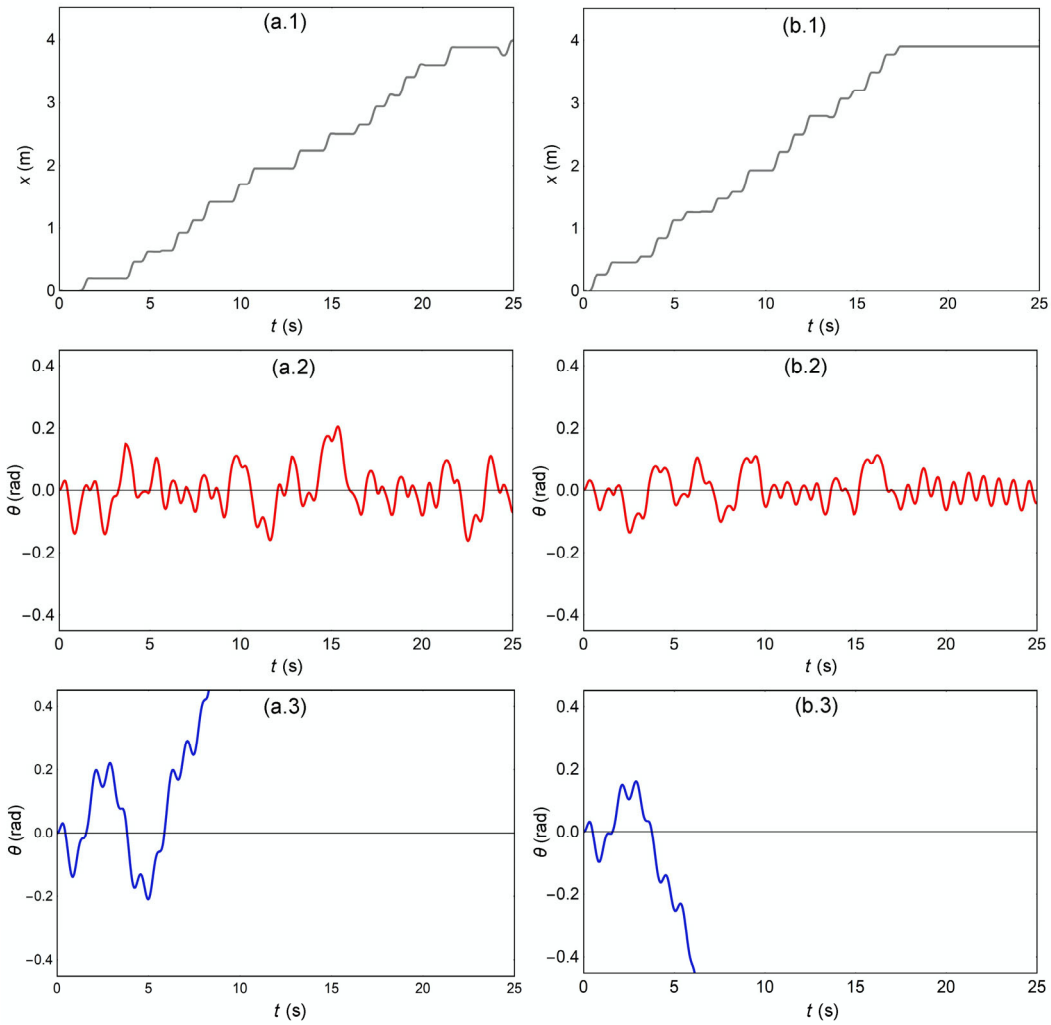

Fig. 10 Behaviour of the flat block (a.1, b.1), the stacked slender block (a.2, b.2), and the slender block alone (a.3, b.3) for varying B/H in the case of very slender blocks

succession. In these two analyzed cases, related to low slenderness, the interposition of the flat pedestal does not change significantly the response of the upper block. A different behaviour can be observed in the case of very slender blocks (Fig. 10), where the overturning of the upper block is avoided with the

squat rigid block at the base.

As can be seen, in both cases the oscillations of the upper block begin before the sliding of the flat one and last for all the time of observation. The sliding motion of the flat block presents a time delay at the beginning and several rest intervals during the observation time. In Fig. 10, the same indications as Fig. 9 are shown: the graphs (a.1) and (b.1) represent the displacements of the flat block, the graphs (a.2) and (b.2) indicate the rotation of the slender one in the case of combination with the pedestal, and the graphs (a.3) and (b.3) indicate the rotation of the slender one in the case of a single rocking block.

In Figs. 11 and 12 the influence of the variation of the upper block mass has been analyzed for a fixed aspect ratio of the block, as can be deduced from the graphs (a.3) and (b.3) in both figures. The rocking of the single block without pedestal is in fact the same in these four cases and is compared with the behaviour of the same block in the presence of the pedestal. In Fig. 11 (lower values of m_2) the flat pedestal only has the effect of retarding the overturning of the upper block, while in the cases of increasing mass (Fig. 12) the overturning is avoided by interposing the pedestal.

4 Conclusions

The real situation of a marble statue placed on a squat rigid base freestanding on a moving floor is presented. A freestanding object may in fact enter a rocking state which would cause overturning due to

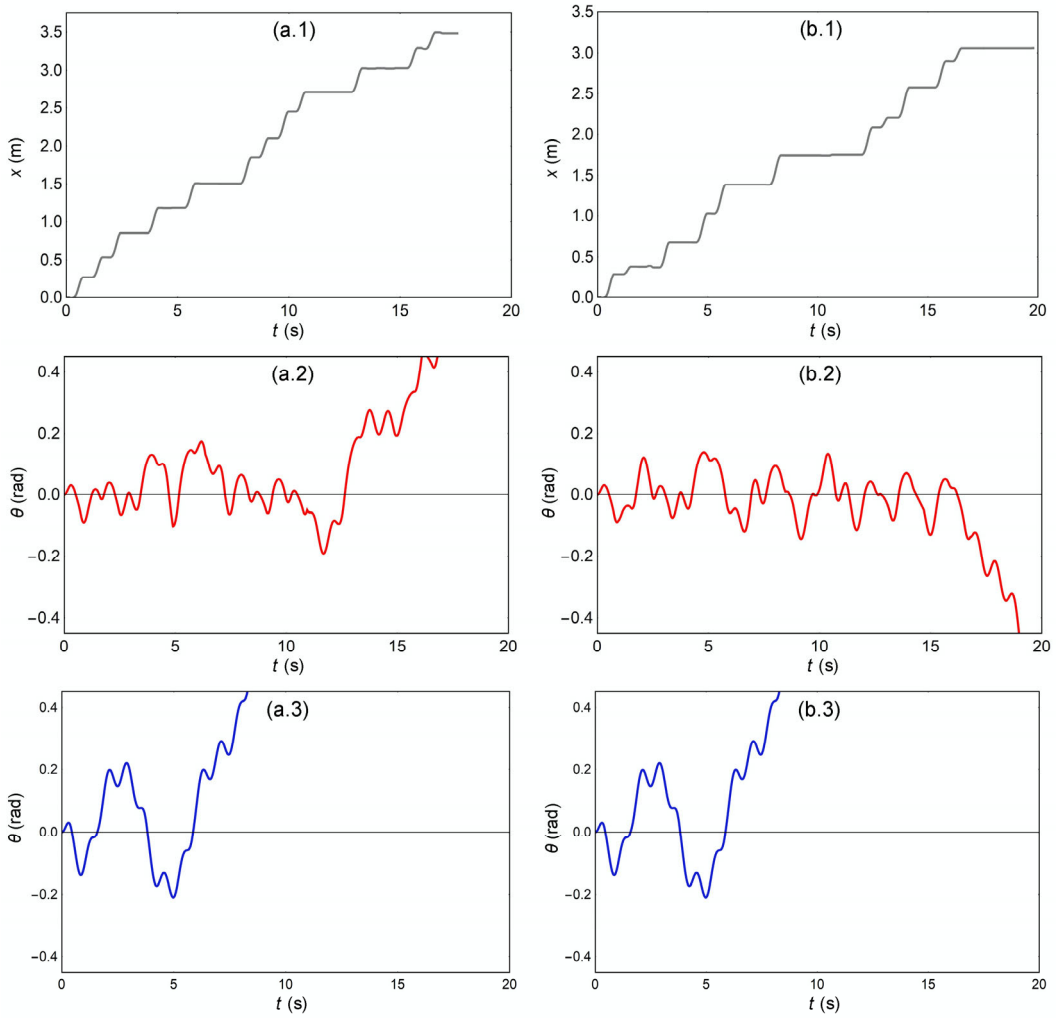

Fig. 11 Behaviour of the flat block (a.1, b.1), the stacked slender block (a.2, b.2), and the slender block alone (a.3, b.3) for varying m_2

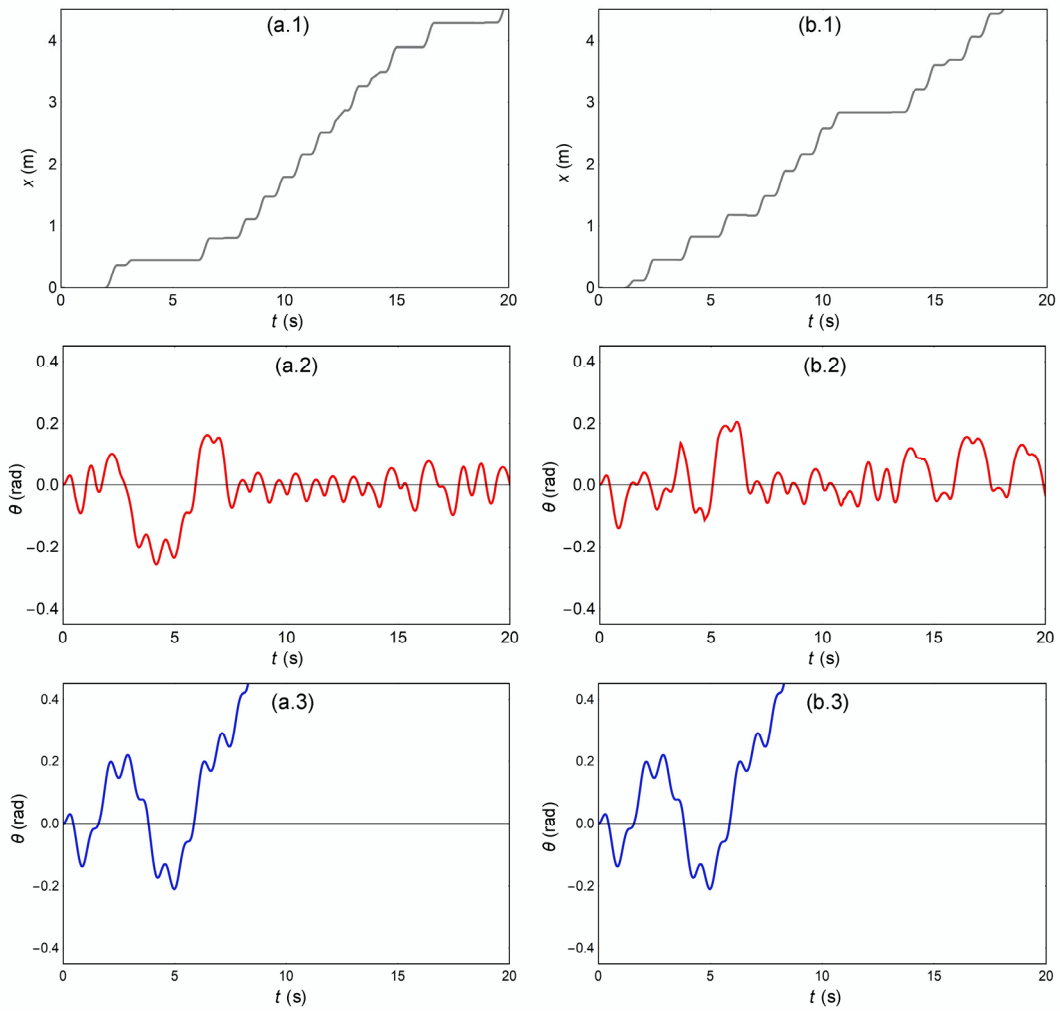

Fig. 12 Behaviour of the flat block (a.1, b.1), the stacked slender block (a.2, b.2), and the slender block alone (a.3, b.3) for varying m_2 in the cases of increasing mass

seismic excitation. Rocking itself can be a cause of damage so that a sliding motion is more desirable. The motion patterns examined in this paper involve only the sliding motion for the lower flat block and rocking as the only possible motion for the stacked slender block. The sliding of the whole complex of rigid bodies is also considered. The system of differential equations governing the problem has been derived and included in a purpose-built numerical procedure. It has been shown that the presence of a rigid surface delays and in some cases avoids the overturning of a slender rigid artifact. This is true especially for slender rocking blocks, and for increasing mass of the upper block. The numerical analysis can be a tool in the choice of the optimal design of the simple isolation system analyzed.

References

Agbabian MS, Ginell WS, Masri FS, et al., 1991. Evaluation of earthquake damage mitigation methods for museum objects. *Studies in Conservation*, 36(2):111-120. https://doi.org/10.2307/1506335

Aslam M, Scalise DT, Godden WG, 1980. Earthquake rocking response on rigid bodies. *Journal of Structural Division*, 106(2):377-392.

Augusti G, Sinopoli A, 1992. Modelling the dynamics of large block structures. *Meccanica*, 27(3):195-211.

Cennamo C, Gesualdo A, Monaco M, 2017. Shear plastic constitutive behaviour for near-fault ground motion. *Journal of Engineering Mechanics*, 143(9):04017086. https://doi.org/10.1061/(ASCE)EM.1943-7889.0001300

Chierchiello G, Gesualdo A, Iannuzzo A, et al., 2015. Structural modeling and conservation of single columns in archaeological areas. Proceedings of the XIV International Forum 'Le vie dei mercanti', p.2012-2020.

Conte E, Dente G, 1989. An analytical solution for Newmark's

sliding block. *Soils & Foundations*, 29(3):152-156. https://doi.org/10.3208/sandf1972.29.3_152

de Canio G, 2012. Marble devices for the base isolation of the two Bronzes of Riace: a proposal for the David of Michelangelo. Proceedings of the XV World Conference on Earthquake Engineering-WCEE, p.24-28. https://doi.org/10.13140/2.1.2483.9047

de Jong MJ, Dimitrakopoulos EG, 2014. Dynamically equivalent rocking structures. *Earthquake Engineering & Structural Dynamics*, 43(10):1543-1564. https://doi.org/10.1002/eqe.2410

Di Egidio A, Contento A, 2009. Base isolation of slide-rocking non-symmetric rigid blocks under impulsive and seismic excitations. *Engineering Structures*, 31(11):2723-2734. https://doi.org/10.1016/j.engstruct.2009.06.021

Erdik M, Durukal E, Ertürk N, et al., 2010. Earthquake risk mitigation in Istanbul museums. *Natural Hazards*, 53(1): 97-108. https://doi.org/10.1007/s11069-009-9411-2

Gesualdo A, Monaco M, 2015. Constitutive behaviour of quasi-brittle materials with anisotropic friction. *Latin American Journal of Solids and Structures*, 12(4):695-710. https://doi.org/10.1590/1679-78251345

Gesualdo A, Iannuzzo A, Monaco M, et al., 2014. Dynamic analysis of freestanding rigid blocks. Civil-Comp Proceedings.

Gesualdo A, Cennamo C, Fortunato A, et al., 2016a. Equilibrium formulation of masonry helical stairs. *Meccanica*, 52(8):1963-1974. https://doi.org/10.1007/s11012-016-0533-9

Gesualdo A, Iannuzzo A, Guadagnuolo M, et al., 2016b. Numerical analysis of rigid body behaviour. *Applied Mechanics and Materials*, 847:240-247. https://doi.org/10.4028/www.scientific.net/AMM.847.240

Gesualdo A, Iannuzzo A, Penta F, et al., 2017. Homogenization of a Vierendeel girder with elastic joints into an equivalent polar beam. *Journal of Mechanics of Materials and Structures*, 12(4):485-504. https://doi.org/10.2140/jomms.2017.12.485

Guadagnuolo M, Monaco M, 2009. Out of plane behaviour of unreinforced masonry walls. *In*: Protection of Historical Buildings. Taylor & Francis Group, New York, USA, p.1177-1180.

Hogan SJ, 1989. On the dynamics of rigid-block motion under harmonic forcing. *Proceedings of the Royal Society A: Mathematical, Physical and Engineering Sciences*, 425(1869):441-476. https://doi.org/10.1098/rspa.1989.0114

Housner WG, 1963. The behaviour of inverted pendulum structures during earthquake. *Bulletin of the Seismological Society of America*, 53(2):403-417.

Ishiyama Y, 1982. Motions of rigid bodies and criteria for overturning by earthquake excitations. *Earthquake Engineering & Structural Dynamics*, 10(5):635-650. https://doi.org/10.1002/eqe.4290100502

Konstantinidis D, Makris N, 2010. Experimental and analytical studies on the response of a 1/4 scale model of freestanding laboratory equipment subjected to strong earthquake shaking. *Bulletin of Earthquake Engineering*, 8(6):1457-1477. https://doi.org/10.1007/s10518-010-9192-8

Kounadis AN, 2015. On the rocking-sliding instability of rigid blocks under ground excitation: some new findings. *Soil Dynamics and Earthquake Engineering*, 75:246-258. https://doi.org/10.1016/j.soildyn.2015.03.026

Makris N, Vassiliou MF, 2012. Sizing the slenderness of free-standing rocking columns to withstand earthquake shaking. *Archive of Applied Mechanics*, 82(10-11):1497-1511. https://doi.org/10.1007/s00419-012-0681-x

Monaco M, Guadagnuolo M, Gesualdo A, 2014. The role of friction in the seismic risk mitigation of freestanding art objects. *Natural Hazards*, 73(2):389-402. https://doi.org/10.1007/s11069-014-1076-9

Moreau JJ, Panagiotopoulos PD, 1988. Nonsmooth Mechanics and Applications. Springer, Wien, Austria.

Newmark NM, 1965. Effects of earthquakes on dams and embankments. *Géotechnique*, 15(2):139-160. https://doi.org/10.1680/geot.1965.15.2.139

Penta F, Rossi C, Savino S, 2014. Mechanical behavior of the imperial carroballista. *Mechanism and Machine Theory*, 80:142-150. https://doi.org/10.1016/j.mechmachtheory.2014.05.006

Prieto F, Lourenço PB, 2005. On the rocking behaviour of rigid objects. *Meccanica*, 40(2):121-133. https://doi.org/10.1007/s11012-005-5875-7

Psycharis IN, 1990. Dynamic behaviour of rocking two-block assemblies. *Earthquake Engineering & Structural Dynamics*, 19(4):555-575. https://doi.org/10.1002/eqe.4290190407

Psycharis IN, Papastamatiou DY, Alexandris AP, 2000. Parametric investigation of the stability of classical columns under harmonic and earthquake excitations. *Earthquake Engineering & Structural Dynamics*, 29(8):1093-1109. https://doi.org/10.1002/1096-9845(200008)29:8<1093::AID-EQE953>3.0.CO;2-S

Purvance MD, Abdolrasool A, Brune JN, 2008. Freestanding block overturning fragilities: numerical simulation and experimental validation. *Earthquake Engineering & Structural Dynamics*, 37(5):791-808. https://doi.org/10.1002/eqe.789

Shao Y, Tung CC, 1999. Seismic response of unanchored bodies. *Earthquake Spectra*, 15(3):523-536. https://doi.org/10.1193/1.1586056

Shenton HW, 1996. Criteria for initiation of slide, rock, and slide-rock rigid-body modes. *Journal of Engineering Mechanics*, 122(7):690-693. https://doi.org/10.1061/(ASCE)0733-9399(1996)122:7(690)

Sinopoli A, 1997. Unilaterality and dry friction: a geometric

formulation for two-dimensional rigid body dynamics. *Nonlinear Dynamics*, 12(4):343-366. https://doi.org/10.1023/A:1008289716620

Spanos P, Koh AS, 1984. Rocking of rigid blocks due to harmonic shaking. *Journal of Engineering Mechanics*, 110(11):1627-1642. https://doi.org/10.1061/(asce)0733-9399(1984)110:11(1627)

Spanos P, Roussis PC, Politis NP, 2001. Dynamic analysis of stacked rigid blocks. *Soil Dynamics and Earthquake Engineering*, 21(7):559-578. https://doi.org/10.1016/S0267-7261(01)00038-0

Voyagaki E, Mylonakis G, Psycharis IN, 2012. Rigid block sliding to idealized acceleration pulses. *Journal of Engineering Mechanics*, 138(9):1071-1083. https://doi.org/10.1061/(ASCE)EM.1943-7889.0000418

Voyagaki E, Psycharis I, Mylonakis G, 2013. Rocking response and overturning criteria for free standing rigid blocks to single-lobe pulses. *Soil Dynamics and Earthquake Engineering*, 46:85-95. https://doi.org/10.1016/j.soildyn.2012.11.010

Voyagaki E, Psycharis I, Mylonakis G, 2014. Complex response of a rocking block to a full-cycle pulse. *Journal of Engineering Mechanics*, 140(6):04014024. https://doi.org/10.1061/(ASCE)EM.1943-7889.0000712

Wolfram S, 2003. The Mathematica Book. Wolfram Media, Inc., Champaign, USA.

Yim SCS, Chopra A, Penzien J, 1980. Rocking response of rigid blocks to earthquakes. *Earthquake Engineering & Structural Dynamics*, 8(6):565-580. https://doi.org/10.1002/eqe.4290080606

中文概要

题　目： 水平支座上独立式刚性块的摆动模型

目　的： 本研究集中探讨水平支座上独立放置简单叠合的双刚性块的动力学行为，旨在通过构建并求解合适的动力学数值模型以助于设计可广泛适用于博物馆、实验室和医院的保护小型艺术品或装置的隔振系统。

创新点： 1. 研究对象为两个叠合在一起的刚性块，较以往同类问题中的单一刚性块，更具现实意义；2. 同时研究了刚性块的摆动和滑动两类运动模式。

方　法： 1. 基于达朗贝尔原理构建摆动控制方程，分析单刚体情形下的摆动并利用数值手段描述其滑动状态；2. 在分析单刚体的基础上构建双刚体控制方程组并对其进行数值求解。

结　论： 1. 通过研究大理石雕塑置于蹲式刚性基底上且基底独立放置在移动地面上的情形发现，相比于滑动，雕塑自身的摆动是造成其损坏的主要原因；2. 在某些情况下，刚体表面延迟的存在可以避免细长刚性块的翻转，尤其是对于那些细长的摇摆块体以及上部块体质量增加的情形；3. 本文提出的数值分析可以成为优化简易隔振系统的一个有效工具。

关键词： 刚体；隔振；雕塑；摩擦；摇摆动力学